REMOTE SENS. ENVIRON. 49:145–154 (1994)

Monitoring of Environmental Conditions in Taiga Forests Using ERS-1 SAR

Eric Rignot,[*] Jo Bea Way,[*] Kyle McDonald,[*] Leslie Viereck,[†] Cynthia Williams,[†] Phyllis Adams,[†] Cheryl Payne,[†] William Wood,[†] and Jiancheng Shi[‡]

*Synthetic-aperture radar images of a forest site near Manley Hot Springs (64°N, 151°W), Alaska, were collected between August 1991 and December 1991, day and night, every 3 days, at C-band frequency ($\lambda = 5.7$ cm), vertical receive and transmit polarization, by the European Space Agency first Remote Sensing Satellite, ERS-1. During the same period, air and soil temperatures and dielectric and gravimetric moisture properties of the forest canopy and forest floor were monitored in three forest stands dominated, respectively, by black spruce (*Picea mariana*), white spruce (*Picea glauca*), and balsam poplar (*Populus balsamifera*). The calibrated ERS-1 radar backscatter values, $\sigma°$, of the forest stands are shown to exhibit a pronounced temporal pattern, with little separability between tree species. The largest change in $\sigma°$, a 3-dB decrease almost independent of tree species, is observed in early winter when the soil and vegetation freeze. In the summer, temporal fluctuations in $\sigma°$ are about 1–2 dB in magnitude, depending on tree species. Diurnal variations in $\sigma°$ are as large as 2 dB during fall freeze-up, and less than 1 dB in summer and winter. These temporal variations in radar backscatter from the forest are interpreted using the MIMICS radar backscatter model and the* in situ *surface observations as due to changes in the dielectric properties of the forest floor and forest canopy induced by precipitation (summer), drought (fall), and freezing (fall–winter) events. In winter, $\sigma°$ increases across the entire landscape, probably because of volume scattering from large depth hoar ice crystals forming in the snow pack.*

INTRODUCTION

Synthetic-aperture radars (SARs) have considerable potential for monitoring environmental and phenologic conditions in forest ecosystems. Electromagnetic signals at microwave frequencies can penetrate through dense vegetation canopies and top layers of the soil surface to monitor: 1) changes in the dielectric properties of the soil and vegetation, thereby providing information on their liquid water content (e.g., Ulaby et al., 1986); and 2) changes in the geometry and amount of vegetation, thereby providing information on forest types (e.g., Cimino et al., 1986) and on total aboveground biomass (Dobson et al., 1992). With the launch of ERS-1 SAR in 1991 by ESA, we have, for the first time, the opportunity to monitor environmental and phenologic conditions in forest ecosystems from space, over long periods of time, and at a frequent revisit interval. In the northern hemisphere high latitudes, where atmospheric warming with doubled CO_2 concentrations could be most significant compared to other latitudes (e.g., Schlesinger and Mitchell, 1987), the ability to monitor seasonal changes in the physical properties of a forest canopy at microwave frequencies may be an essential tool for assessing the effect or response of the boreal biome to climate change.

During the Commissioning Phase of ERS-1, which extended from 3 August 1991 to 15 December 1991, ERS-1 SAR had a 3-day repeat-orbit cycle which, for some parts of the world, including Alaska, provided an exact repeat coverage of the same areas every 3 days. In addition, day and night radar observations could be obtained repeatedly in the center of Alaska, at the

[*]Jet Propulsion Laboratory, Pasadena, California
[†]Institute of Northern Forestry, Fairbanks, Alaska
[‡]Department of Geography, University of California, Santa Barbara

Address correspondence to Eric Rignot, JPL, California Inst. of Technol., MS 300-243, 4800 Oak Grove Dr., Pasadena, CA 91109.
Received 4 February 1993; revised 6 November 1993.

0034-4257/94/$7.00

655 Avenue of the Americas, New York, NY 10010

crossing of ERS-1 descending and ascending passes, near the city of Manley Hot Springs. We selected a forest study site in that area and monitored the weather and soil and vegetation moisture conditions of the forest in three forest stands dominated by three different tree species. This experiment provided an opportunity to determine the magnitude of temporal changes in ERS-1 radar backscatter of different tree species in response to naturally occurring environmental changes, and determine whether changes in radar backscatter could be related to changes in the structural and electrical properties of the forest canopy and forest floor via relevant scattering mechanisms using radar backscatter models. These observations are needed to determine the potential and limitations of ERS-1 SAR for monitoring forest conditions in interior Alaska and to develop inversion techniques for extracting forest parameters of interest to ecosystem and climate models from the SAR observations.

METHODS

Study Site

The Manley forest site is 40 km downstream from the city of Manley Hot Springs, along the Tanana River, at a center location of 64°52′N and 151°20′W. The forest site includes both upland fire-controlled succession and floodplain succession forests, but the three forest stands we selected are in the floodplains. Upland forests vary from highly productive aspen (*Populus tremuloides*), paper birch (*Betula papyrifera*), and white spruce (*Picea glauca*) stands on south-facing, well-drained slopes, to permafrost and moss-dominated black spruce (*Picea mariana*) forests of low productivity on north-facing slopes (Viereck et al., 1983). In the floodplain, the active erosion of mature stands along the Tanana and production of silt bars on the river floodplains yield forest stands in a variety of young successional stages (Van Cleve and Viereck, 1981). Primary succession begins with willow and alder shrubs (*Alnus tenuifolia*), which act to slow the river flow, stabilize the terraces, and provide biological control allowing the forest floor to develop. Alder and willow shrubs are followed by balsam poplar (*Populus balsamifera*), which competes with the shade-intolerant shrubs. When sufficient alluvium has accumulated to raise river terraces above the zone of frequent intraseason flooding, white spruce slowly becomes dominant. In locations where the white spruce stands are protected from erosion, their shading allows the formation of permafrost which eventually results in a transition to slow-growing black spruce and bogs.

Climatic conditions at the Manley forest site are similar to those in Fairbanks. In the Fairbanks area, the climate is continental, with large diurnal temperature changes, low precipitation, low cloud cover, and low humidity (Slaughter and Viereck, 1986). January is the coldest month with a mean daily temperature of −25°C; and July is the warmest with a mean daily temperature of +16°C. Mean annual temperature is −3.5°C, and temperature extremes range from +35°C in June to −65°C in January. The annual mean precipitation is 286 mm, with about 30% falling as snow. Rainfall occurs mostly in July and August, with the heaviest and most frequent precipitation in August. Snow generally covers the entire landscape from October through mid-April. Maximum snow accumulation is 75–100 cm at Fairbanks.

ERS-1 SAR Data

ERS-1 SAR operates at C-band frequency ($\lambda = 5.7$ cm), vertical transmit and receive polarization, and 23° look angle (Attema, 1991). As ERS-1 SAR does not carry an on-board data recorder, SAR data can only be received in view of a receiving station. The data described in this article were received and processed at NASA's Alaska SAR Facility (ASF), University of Alaska, Fairbanks, Alaska (Carsey and Weeks, 1987). The SAR scenes are 100 km × 100 km in size, 4-looks in azimuth, 1-look in range, 12.5 m pixel spacing in both slant-range and azimuth, and 30 m resolution on the ground. Images acquired during descending passes of the satellite correspond to daytime passes at 1:00 pm Alaska daylight time; ascending passes correspond to nighttime passes at 1:00 am Alaska daylight time. The SAR data are calibrated with an absolute calibration accuracy better than 1 dB (Fatland and Freeman, 1992), and a temporal stability of the calibration better than 0.33 dB (Attema, 1991; 1992). ERS-1 SAR is a suitable tool for monitoring studies as changes in radar backscatter can be detected at the 0.5 dB level with confidence.

During the 3-day repeat-orbit cycle, each point of a SAR scene was imaged at the same time of the day (within a few minutes), and with the same incidence angle of the radar illumination (within fractions of a degree). Because the imaging geometry remains the same, temporal changes in radar backscatter can be directly analyzed using slant-range SAR imagery, that is, without requiring computationally expensive geometric correction routines, resampling, and georeferencing of the SAR images. Registration of repeat-pass, slant-range, SAR images on a pixel to pixel basis only requires the selection of one tie-point (Rignot and van Zyl, 1993). Daytime and nighttime data are registered independently because of differences in imaging geometry between descending and ascending passes. Polygons drawn on the computer for each forest stand are used to extract the ERS-1 pixel values from the registered SAR images, convert them into calibrated radar backscatter intensities, and average them over the whole stand to obtain a mean value that is not affected by speckle noise. For each stand, the number of pixels is

larger than 2200 pixels, yielding a contribution of image speckle to the variance to mean square ratio of the average radar backscatter values less than 0.1%.

Ground Truth

The three forest stands are labeled BS-50 (black spruce), BP-51 (balsam poplar), and WS-52 (white spruce) (Fig. 1). Their location was selected using infrared aerial photos prior to ground sampling and extraction of radar backscatter values. An additional treeless stand (SH-51) was selected in the open, although no *in situ* measurements were made at that location, to compare the radar backscatter values recorded in treeless areas to those recorded in forested areas.

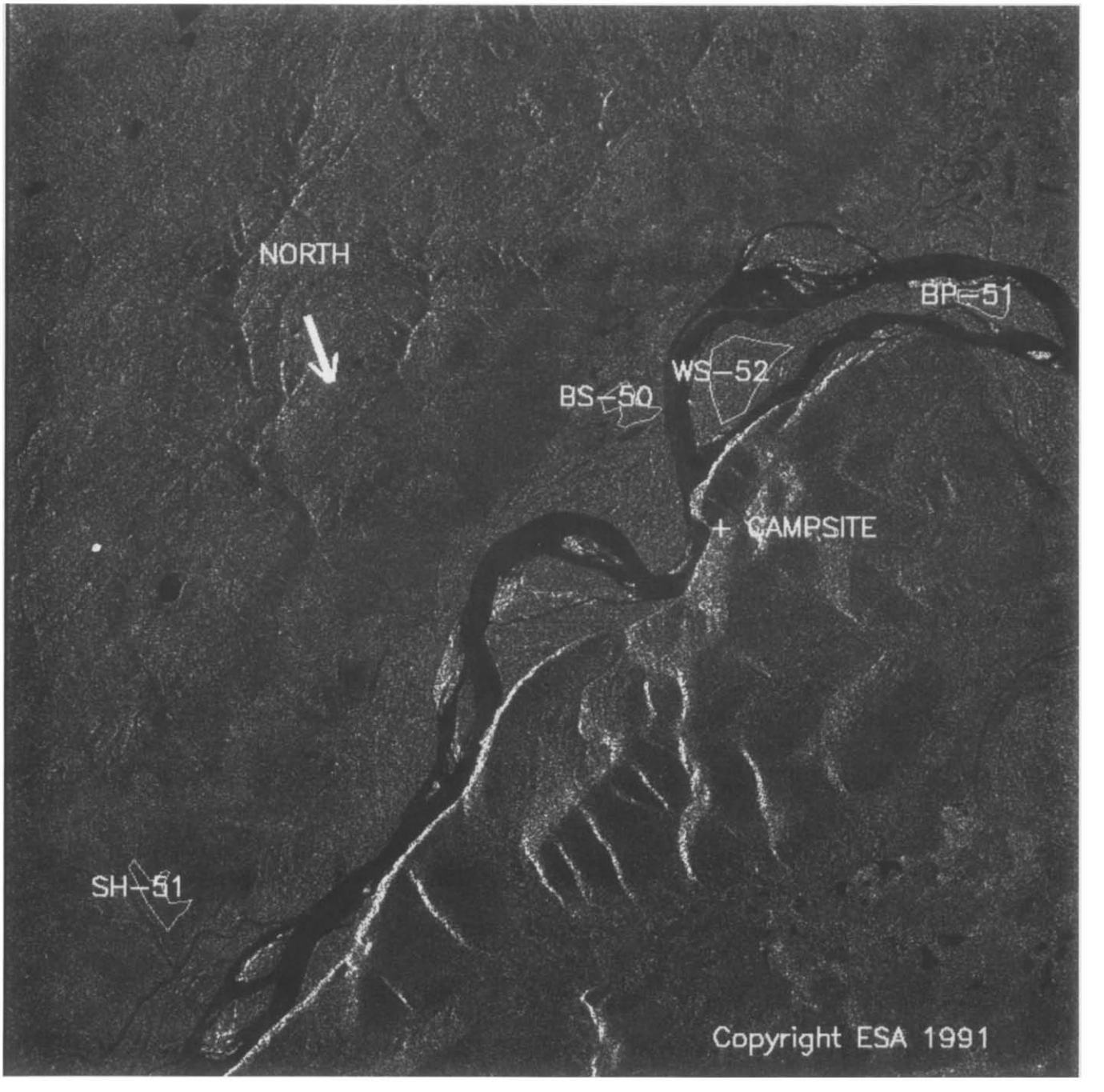

Figure 1. ERS-1 SAR image of the Manley forest site acquired on DOY 224 (12/08/91) during a descending/day pass, and location of the three monitored forest stands along the Tanana river. BS-50 is black spruce, BP-51 is alsam poplar, WS-52 is white spruce, and SH-51 is a treeless area of bog/fen vegetation. ERS-1 is flying from bottom to top in the figure, looking to its right, heading south. The image is 1536 × 1536 pixels in size, corresponding to a 16 km × 16 km region. © ESA 1991.

Static Properties

Tree diameter at breast height (DBH), tree height, stem density, tree age, tree species composition, and understory ground cover description were collected in the three forest stands along a single transect crossing the center of each stand. Infrared, aerial photos were used to select the transect starting points and direction for each stand. Each transect included 10 sampling plots typically separated by 100 m except in the presence of anomalous vegetation (such as found in old sloughs). Plot radii were chosen to include at least 15 trees with a DBH of at least 2.5 cm. The results show that black spruce exhibits the greatest density (Table 1), but contains less woody material than the other forest stands because of the smaller tree size.

Within Stand Weather Data

Weather data were recorded in three forest stands using an Easylogger data logger with an Eprom data storage pack, a quantum PAR sensor, a Physchem temperature / relative-humidity, and three direct burial soil temperature probes. A rain gauge was placed in the open near the campsite (Fig. 1). Figure 2c shows the air temperatures recorded in BS-50. Soil temperatures recorded in BS-50 (not shown in Fig. 2) indicate that the soil was frozen to 10 cm depth on DOY (day of year) 280 and remained so for the rest of the period of observation.

Airport Weather Data

Weather data from the Tanana airport at the western edge of the swath include visual observations, minimum–maximum air temperatures, daily precipitation rates, and snow depth. The air temperatures recorded at Tanana airport are similar to those observed in BS-50. The daily precipitation rates and snow depths recorded at Tanana are shown in Figures 2d and 2e.

Temporally Varying Canopy and Soil Properties

Temporally varying properties include dielectric constant profiles of the tree trunks, and gravimetric moisture content of the forest canopy and forest floor. The dielectric constant of the tree trunks was measured in each stand in the bark, phloem, cambium, and xylem, corresponding to a depth of the dielectric probe inside the bole of about 0 cm, 0.3 cm, 0.6 cm, and 1.6 cm, respectively. Each measurement set was preceded by calibration with alcohol and water. An average value was computed from four measurements made on three different trees. Within the relatively large standard error of the average measurements (30–40%), the results show almost no variation in the dielectric properties of the tree trunks during the period of *in situ* moisture measurements, which extended from DOY 218 to DOY 251.

Samples of the leaves / needles, branches, outer-bole (bark and phloem), inner-bole (cambium and xylem), and understory (shrubs), litter, moss, organic soil, and mineral soil were collected and weighed in the field, carried back to the laboratory by plane, dried in the oven, and weighted again to compute their gravimetric moisture content expressed in percentage of the dry weight. The results are shown in Table 2 for BS-50, BP-51, and WS-52 on four different dates. Each point

Table 1. Forest Stand Characteristics used by MIMICS[a]

Properties	*Black Spruce*	*White Spruce*	*Balsam Poplar*
Trunk layer properties			
Mean height (m)	5.1	16.7	20.1
Mean diameter (cm)	6.5	21.3	22.5
Stem density (stems/m^2)	0.137	0.0654	0.106
Crown layer properties (leaf-needle)			
Canopy thickness (m)	5.1	14.7	10.1
Mean length (cm)	0.8	1.6	6.8
Mean thickness/diameter (cm)	0.1	0.1	0.03
Density (leaf-needle/m^3)	12456	12300	98.1
Orientation [uniform = 0.5 sin(φ)]	0.5 sin(φ)	0.5 sin(φ)	0.5 sin(φ)
Primary branches			
Mean length (m)	0.62	1.13	2.0
Mean diameter (cm)	1.81	2.24	1.5
Density (branches/m^3)	0.25	0.44	0.85
Orientation	$\sin^9(\theta - 30°)$	$\sin^4(\theta)$	$\sin^9(\theta + 60°)$
Secondary branches			
Mean length (m)	0.39	0.57	1.0
Mean diameter (cm)	0.81	1.04	0.75
Density (branches/m^3)	1.31	2.37	6.69
Orientation	$\sin^9(\theta)$	$\sin^9(\theta)$	$\sin^9(\theta + 60°)$
Ground characteristics used by MIMICS			
rms height (cm)	0.17	0.25	1.0
Correlation length (cm)	2.0	2.0	4.0
Surface model (SP = small perturbation)	SP	SP	SP

[a] The trunk layer properties are means of 10 plots with more than 15 trees per plot.

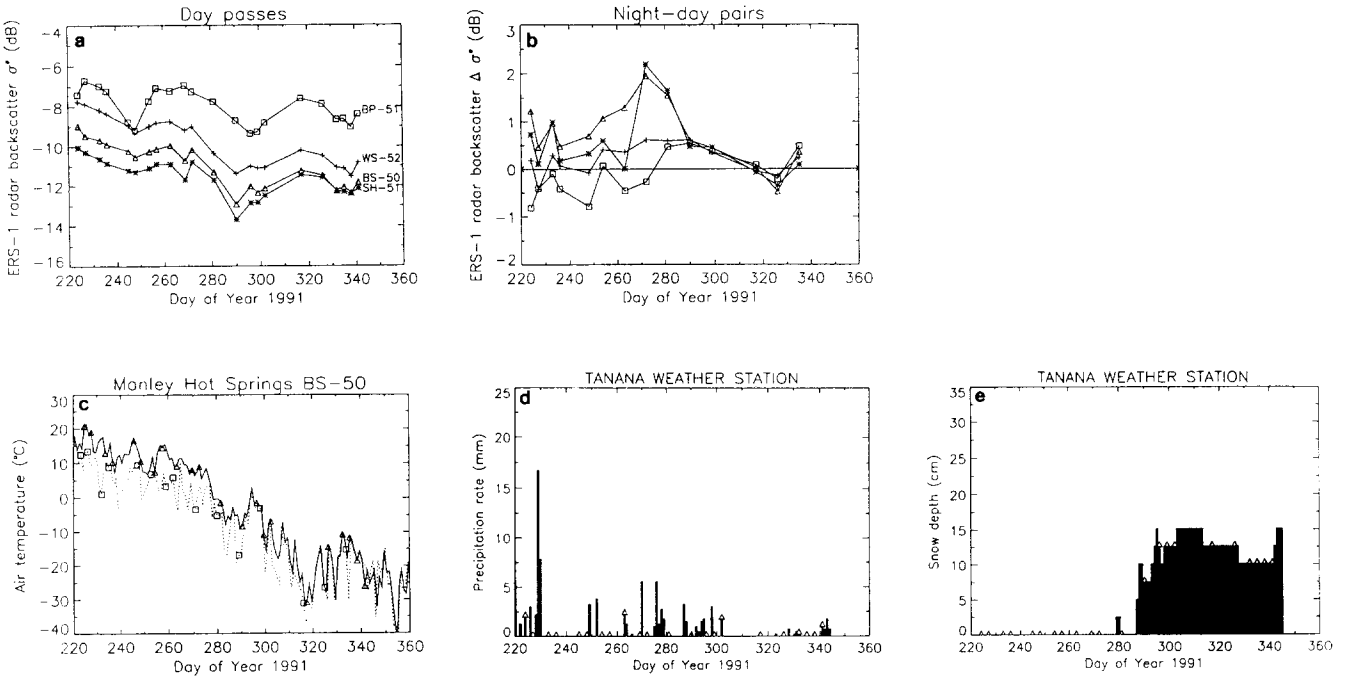

Figure 2. a) ERS-1 radar backscatter values for BS-50 (triangle), BP-51 (square), WS-52 (vertical cross), and SH-51 (star) during descending / daytime passes. b) Changes in radar backscatter between ascending / nighttime and descending / daytime passes ($\Delta\sigma^\circ > 0$ means σ° is higher during the day). Night-time passes are 12 hours prior to day-time passes. (c) Air temperature (°C) in BS-50 during the day (continuous line) and at night (dotted line) vs. day of year. d) Daily precipitation rates (mm) recorded at Tanana vs. day of year. (e) Snow depth (cm) recorded at Tanana vs. day of year. Triangles in c,d, and e indicate the dates of availability of ERS-1 SAR data during a daytime pass. Squares in c) indicate the dates of availability of ERS-1 SAR data during a nighttime pass.

Table 2. Gravimetric Moisture Content Measurements Expressed in Percentage of Dry Weight in a) BS-50, b) WS-52, and c) BP-51[a]

Day of Year	*224*	*227*	*233*	*248*
a) Moisture content (g/g in %)				
Needles	56.3 ± 1.7	54.1 ± 0.5	53.1 ± 2.7	52.9 ± 0.9
Branches	51.4 ± 3.7	44.0 ± 2.8	43.0 ± 2.0	44.1 ± 2.0
Bark-phloem	45.8	37.4	30.9	34.2
Cambium-xylem	36.3	41.0	39.0	35.2
Understory	59.3	51.9	48.2	43.4
Moss	87.3 ± 2.3	81.9 ± 2.0	74.1 ± 9.3	35.6 ± 23.8
Litter	63.0 ± 5.7	48.0 ± 7.9	38.6 ± 2.4	17.7 ± 6.9
Organic soil	62.7 ± 7.4	65.8 ± 6.3	71.5 ± 14.3	69.1 ± 10.3
Mineral soil	52.9 ± 3.2	58.4 ± 1.3	67.0 ± 6.5	57.6 ± 4.1
b) Moisture content (g/g in %)				
Needles	55.8 ± 5.1	58.3 ± 1.7	58.2 ± 0.5	57.2 ± 2.8
Branches	59.1 ± 12.7	46.6 ± 12.7	50.6 ± 4.3	49.4 ± 4.6
Bark-Phloem	47.7	43.5	44.9	44.6
Cambium-Xylem	50.2	58.5	54.2	52.0
Understory	74.2	64.4	61.8	59.2
Moss	62.9 ± 8.2	68.7 ± 1.4	57.2 ± 2.5	9.5 ± 4.1
Litter	51.0 ± 8.7	53.5 ± 7.1	35.4 ± 5.3	15.1 ± 2.8
Organic soil	62.1 ± 12.2	50.7 ± 11.6	43.7 ± 12.4	43.2 ± 1.9
Mineral soil	33.6 ± 1.3	35.7 ± 2.2	36.2 ± 5.7	22.3 ± 4.3
c) Moisture content (g/g in %)				
Leaves	56.8 ± 0.6	64.3 ± 2.8	64.6 ± 1.9	60.9 ± 4.0
Branches	55.5 ± 8.2	48.5 ± 0.6	47.5 ± 2.4	45.8 ± 1.2
Bark-Phloem	46.0	38.1	35.9	36.2
Cambium-Xylem	54.3	47.8	51.0	47.3
Understory	69.7	67.2	71.3	54.7
Litter	48.2 ± 0.8	44.0 ± 2.6	46.2 ± 8.9	7.0 ± 2.0
Organic soil	50.1 ± 11.7	60.9 ± 3.2	62.1 ± 7.6	28.0 ± 0.7
Mineral soil	35.1 ± 1.3	18.1 ± 5.6	21.9 ± 6.0	15.7 ± 3.8

[a] The standard deviations of the measurements are indicated with a ± sign. Moss is not present in BP-51.

is the average of one measurement made at four locations. As the number of samples is quite low, these measurements do not provide a complete characterization of the soil and vegetation moisture conditions over the entire stand. Nevertheless, the results suggest that the moisture content of the leaves / needles, branches, outer-bole, and inner-bole remained high during the period of observation, with little temporal variability, while the moisture content of the shrubs, litter, moss, and (to a lesser extent) organic soil decreased by more than 80% between DOYs 224 and 248 in all forest stands. Hence, between DOYs 218 and 251, the moisture conditions changed quite significantly in the forest floor, but not so much in the forest canopy.

Microwave Modeling

The Michigan microwave canopy scattering model (MIMICS) (Ulaby et al., 1990) is used to model the radar backscatter from various tree species using the ERS-1 SAR imaging conditions. The forest canopy is modeled as two distinct horizontal vegetation layers comprised of leaves, branches, and tree trunks, over a dielectric ground surface. The model requires both static (structure and geometrical characteristics) and dynamic (moisture content) properties of the soil and vegetation. The static properties of the forest canopy used in the model are shown in Table 1. The DBH, height, and stem density values were measured at the Manley forest site. The needles, leaves, branches, and ground input static characteristics were estimated from a database of measurements collected in earlier experiments, in similar stands, at the Bonanza Creek Experimental Forest (Way et al., 1990). For each forest stand, the forest floor is modeled as an electromagnetically equivalent bare surface whose roughness characteristics are given in Table 1.

We simulated the ERS-1 σ° for a range of soil and vegetation moisture conditions to determine the magnitude of the different scattering components contributing to the total radar backscatter, and to estimate the sensitivity of σ° to the water status of the soil and vegetation as predicted by MIMICS. The results help interpret the ERS-1 observations, and predict changes in radar backscatter that could be observed during the rest of the year. In the simulation, the volumetric soil moisture varies between 5% (very dry or frozen soil; Wegmüller, 1990) and 35% (wet soil), corresponding to a dielectric constant of the soil varying between $\varepsilon = 3.3 - j\,0.7$ and $\varepsilon = 18.8 - j\,4.5$. The dielectric constant of the woody material (tree trunks, branches) varies between $\varepsilon = 4.6 - j\ 1.4$ (frozen tree; Way et al., 1990) and $\varepsilon = 29.7 - j\ 9.4$ (flooded tree). Leaves and needles are assumed to have the same dielectric properties as wood. The dielectric constant of the vegetation is computed using Ulaby and El-Rayes's (1987) model with a dry wood density of 0.37. For the soil, we use Hallikainen et al.'s (1985) model with a soil texture of 10% sand and 30% clay.

Figure 3a show that σ° may vary by as much as 6 dB with varying forest floor conditions, and by less than 3 dB with varying moisture conditions of the forest canopy. Similar results are obtained for WS-52 and BP-51, although in the latter case the sensitivity to moisture conditions of the forest canopy is less. Hence, the moisture conditions of the forest floor play an important role in the dynamics of the radar backscatter values from the forest. Increasing the moisture content of the forest floor and increasing the moisture content of the forest canopy both increase σ°, suggesting that changes in σ° recorded by ERS-1 are positively correlated with changes in the dielectric properties of the soil and vegetation considered as a single medium, assuming no loss of plant material and no change in the ground static characteristics.

Calculations of the relative magnitude of contributions to σ° from different scattering paths show that direct scattering from the ground is important in sparse, open canopies in all conditions, and in frozen canopies for all tree species (Figs. 3d–f). Scattering from the crown is never a factor in black spruce, but is important in white spruce and balsam poplar. Other scattering paths such as ground–crown ground, crown–ground, and ground–crown interactions are of second-order magnitude in all circumstances. Trunk–ground interactions dominate when the soil and vegetation are wet. The magnitude of these interactions may, however, be overestimated in the MIMICS model, which assumes that the ground acts as a perfectly smooth dielectric reflector during trunk–ground interactions while the forest floor, which comprises a dense understory vegetation, may actually significantly attenuate the incoming radar signals (unless flooded).

RESULTS

ERS-1 Observations

The radar backscatter curves from the three forest stands show pronounced temporal variations during the period of observation (Fig. 2a). σ° is highest in the summer, reaching a low minimum in fall when air-temperatures are several degrees below zero, and increasing again in winter. The separability in radar backscatter between tree species is typically small and less than 2 dB. The radar backscatter curves from BS-50, WS-52, and SH-51 follow similar trends from August to December, but BP-51 follows a different trend in the summer. Diurnal variations in σ° are large in fall, small in summer, and miminum in winter.

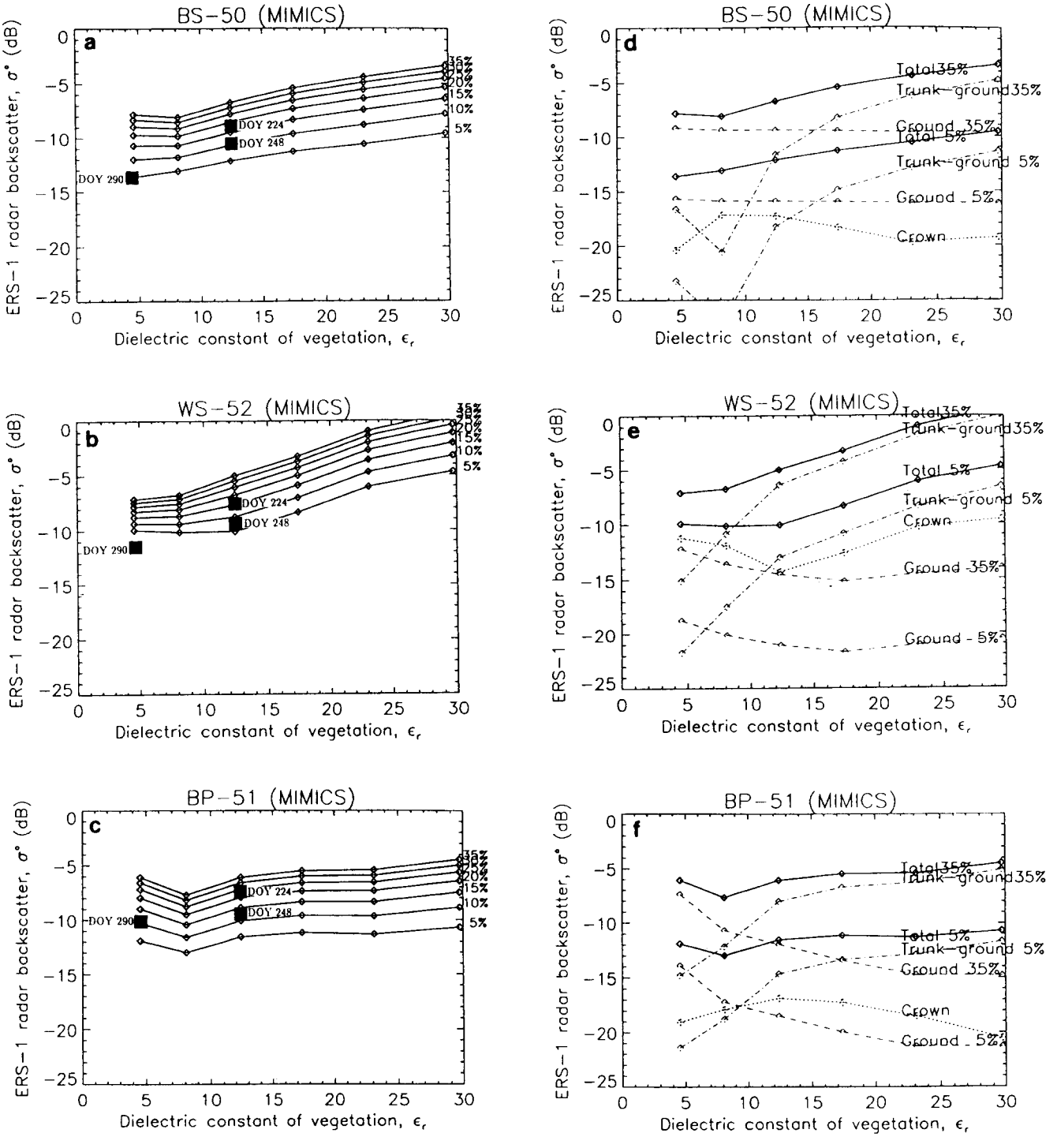

Figure 3. ERS-1 radar backscatter values predicted by MIMICS vs. the real part of the dielectric constant of the woody material ε_r for different values of the volumetric moisture content of the soil in a) BS-50, b) WS-52, and c) BP-51. Contributions to the total radar backscatter (solid line) of three dominant scattering mechanisms with wet soil (soil moisture = 35%) and dry soil (soil moisture = 5%) conditions for d) BS-50, e) WS-52, and f) BP-51. Direct scattering from the crown does not depend on the ground conditions. Black squares in a), b), and c) indicate the radar backscatter values measured by ERS-1 on three different dates: DOYs 224, 248, and 290. On those dates, the dielectric constant of the forest canopy is estimated from the *in situ* observations using Ulaby and El-Rayes's (1987) model.

ERS-1 Observations versus Weather Conditions

Between DOYs 220 and 230, the canopy and forest floor are wet in all forest stands due to heavy rain showers prior to DOY 220 (precipitation rate is 38 mm on DOY 215), and $\sigma°$ is the highest of the period of observation (Fig. 2a). Between DOYs 231 and 250, there are no precipitation (Fig. 2d), the moisture content of the leaves, branches, and trunks remains high, the moisture content of the forest floor decreases significantly (Table 2), and $\sigma°$ decreases by 1 dB in BS-50, WS-52, and SH-51, and by 2 dB in BP-51. Wet conditions return on DOY 250, and $\sigma°$ increases by 1 dB in coniferous trees, and 2 dB in deciduous trees.

Snow appears on DOY 279 (Fig. 2e) along with day-time subzero air temperatures (Fig. 2c), following 4 days of wet (precipitation averages 3 mm per day between DOYs 275 and 278) and cold (air temperature averages 5°C) conditions. The snow cover reduces to traces between DOYs 281 and 286, and reaches 5 cm again on DOY 287 and 10 cm on DOY 288. During that period, $\sigma°$ decreases by 3 dB to reach a low minimum on DOY 290 for BS-50 and WS-52 and on DOY 296 for BP-51. The decrease in $\sigma°$ suggests a large decrease in the dielectric properties of the soil and vegetation, induced by dry climatic conditions between DOYs 271 and 274 (Fig. 2d), followed by freezing conditions on DOY 279 (Fig. 2c, soil temperature of -0.4°C at 10 cm depth in BS-50).

After DOY 290, snow depth is greater than 10 cm, and $\sigma°$ increases with time until DOY 341. Vigorous freezing is expected to stabilize $\sigma°$ from the forest because nearly all the fresh liquid water content inside the soil and vegetation is frozen, and the dielectric constant of the soil and vegetation reaches a low minimum. Similarly, changes in radar backscatter due to the greater penetration depth of the radar signals inside the forest canopy (the imaginary part of the dielectric constant is lower) are not expected to yield such large changes in radar backscatter from the forest (Fig. 3), and to extend over such long periods of time as observed by ERS-1 (Fig. 2a). Fresh fallen snow itself has little effect on $\sigma°$. Using a two-layered radiative transfer model for snow, with spherical snow grains 0.5 mm in diameter, 0.40 g/cm^3 in density, at a temperature $T = -5$°C, we predict that $\sigma°$ due to scattering from fresh, dry snow grains under ERS-1 imaging conditions is about -15 dB (Fig. 4), that is, several dB below the $\sigma°$ values recorded for the forest, so that fresh snow is nearly transparent to the radar signals. On the other hand, Alaskan snow undergoes rapid, and dramatic structural changes in winter with the growth of depth hoar crystals at the base of the snow pack. Low air temperatures ($T < -20$°C) combined with warm snow/ground interface temperatures ($T > -5$°C) create strong vertical temperature gradients across a relatively thin

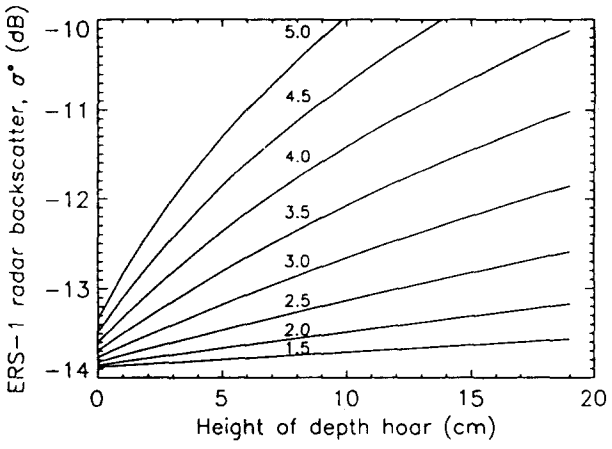

Figure 4. Radar backscatter of snow at C-band frequency, VV-polarization, 23° look angle, using a two-layered radiative transfer model of snow above a bare surface. The underlying ground surface has an rms height of 0.5 cm and a correlation length of 2 cm. The air–snow interface has an rms height of 0.125 cm and a correlation length of 1.5 cm. Snow grains in the upper layer are spheres 0.5 mm in diameter, 0.46 g/cm^3 in density, at a temperature of -5°C. The bottom snow layer is a layer of depth hoar crystals of coarser grain diameter. $\sigma°$ is plotted for different diameters of the depth hoar ice crystals vs. the height of the depth hoar layer, keeping the total height of the snow pack (fresh snow + depth hoar) constant and equal to 20 cm.

layer of dry, cold, and porous snow, which results in the transport of water vapor from the ground into the snow pack which directly crystallizes to form coarse, hollow, skeletal ice crystals (e.g., Traband and Benson, 1972; Sturm and Johnson, 1992). Depth hoar crystals develop rapidly in early winter, growing up to 30 mm in length at the base of the snow with an average grain size diminishing with height, and occupying almost the entire snow cover by midwinter. Past studies have shown that depth hoar crystals are efficient volume scatterers that can significantly lower the emissivity of the snow pack at microwave frequencies (e.g., Hall et al., 1991). Using a two-layered radiative transfer model for snow above a frozen ground, we estimated the effect of depth hoar crystals on ERS-1 $\sigma°$. The free parameters are the diameter of the depth hoar crystals (assumed spherical) and the height of the depth hoar layer relative to the total height of the snow layer. The results, shown in Figure 4, illustrate that depth hoar crystals with an effective diameter of 2.5–3.5 mm, and a depth hoar height increasing from 0 cm to 15 cm, can easily account the 2 dB increase in $\sigma°$ observed by ERS-1, which we therefore attribute to volume scattering from the snow.

Diurnal variations in $\sigma°$ are largest on DOY 272 in BS-50 and SH-51 when air temperatures go from several degrees below zero at night to well above zero during the day. At the same time $\sigma°$ changes by less than 0.5

dB in WS-52 and BP-51, perhaps revealing that freezing temperatures did not affect trees as much as the ground floor layers. After DOY 300, changes in $\sigma°$ are less than 0.5 dB, consistent with the fact that trees and ground layers are already frozen during daytime passes.

ERS-1 Observations versus Phenologic Changes

Changes in radar backscatter with leaf fall are not separable from changes due to environmental conditions (Fig. 2a), probably because they occur on a longer time-scale: Leaves are browning/yellowing on DOY 239, all yellow on DOY 247, half fallen on DOY 251, and all fallen on DOY 269. After DOY 270, however, the temporal pattern in $\sigma°$ exhibited by leafless BP trees resembles that exhibited by conifers, whereas important differences exist in the summer and fall (Fig. 2a). These observations are consistent with the MIMICS prediction that crown scattering dominates in the presence of leaves when the soil and vegetation are wet, while scattering from the forest floor dominates in the absence of leaves when the soil and vegetation are dry or frozen.

ERS-1 Observations versus MIMICS Predictions

The ERS-1 and *in situ* observations indicate that the moisture status of the forest floor has a major influence on the temporal radar backscatter response from the forest, despite attenuation of the radar signals through the forest canopy. In the current version of MIMICS, the forest floor is modeled as an electromagnetically equivalent bare surface. Understanding this limitation, we adjusted the rms height and correlation length of the bare surface in the simulation to obtain radar backscatter values within the range of those measured by ERS-1. For BS-50, the model predictions compare very well with the ERS-1 observations on three different dates (Fig. 3a); for WS-52 and BP-51, the predictions are within 2 dB of the observations (Fig. 3b–c). Nevertheless, for all three stands, the predicted trend in radar backscatter from the forest is consistent with the ERS-1 observations and the *in situ* measurements, and MIMICS provides invaluable insight in the scattering mechanisms responsible for the radar backscattering characteristics of the forest.

CONCLUSIONS

The first spaceborne, calibrated, radar observations of an Alaskan forest ecosystem recorded by ERS-1 show that pronounced temporal variations in radar backscatter are detected during summer–fall–winter transitions, with the largest changes occurring during transitions from warm and wet conditions to frozen and dry conditions. These changes are interpreted using the MIMICS radar backscatter model and *in situ* surface observations as induced by large changes in the dielectric properties of the forest floor and forest canopy. These results are encouraging that ERS-1 could play a significant role in the monitoring of moisture conditions in forest ecosystems, and thereby provide complementary information to that obtained from passive sensors operating at optical wavelengths. Changes in the structure of the forest canopy associated with the loss of the plant material are less apparent and require further study, whereas structural changes in the snow pack are clearly detected by ERS-1.

We would like to thank the people from the Alaska SAR Facility, University of Fairbanks, Alaska, for receiving, processing, calibrating, and archiving the ERS-1 SAR data. This work was carried out at the Jet Propulsion Laboratory, California Institute of Technology, under contract with the National Aeronautics and Space Administration.

REFERENCES

Attema, E. (1991), The active microwave instrument on-board the ERS-1 satellite, *Proc. IEEE* 79:791–799.

Attema, E. (1992), Science requirements for the calibration of the ERS-1 synthetic aperture radar, *Proc. CEOS SAR Calibration Workshop*, Ottawa, Canada, 21–25 Sep. 21–25.

Carsey, F., and Weeks, W. (1987), The planned Alaska SAR Facility: an overview, in *Proc. of the 1987 Int. Geosci. and Remote Sens. Symp.*, IEEE Cat. 87CH2434-9, Ann Arbor, MI, 18–21 May, pp. 1059–1062.

Cimino, J. B., Brandani, A., Casey, D., Rabassa, J., and Wall, S. (1986), Multiple incidence angle SIR-B experiment over Argentina: mapping of forest units, *IEEE Trans. Geosci. Remote Sens.* 24:498–509.

Dobson, C., Ulaby, F. T., LeToan, T., Beaudoin, A., Kasischke, E. S., and Christensen, N. (1992), Dependence of radar backscatter on coniferous biomass, *IEEE Trans. Geosci. Remote Sens.* 30:412–415.

Fatland, R., and Freeman, A. (1992), Calibration and change detection using Alaska SAR Facility ERS-1 SAR data, *Proc. of the 1992 Int. Geosci. and Remote Sens. Symp.*, IEEE Cat. 92CH3041-1, Houston, TX, 26–29 May, pp. 1164–1166.

Hall, D. K., Sturm, M., Benson, C. S., et al. (1991). Passive microwave remote and *in-situ* measurements of Arctic and subarctic snow covers in Alaska, *Remote Sens. Environ.* 38: 161–172.

Hallikainen, M., Ulaby, F. T., Dobson, M. C., El-Rayes, M., and Wu, L. K. (1985), Microwave dielectric behavior of wet soil-part I: Empirical models and experimental observations, *IEEE Trans. Geosci. Remote Sens.* 23:25–34.

Rignot, E., and van Zyl, J. J. (1993), Change detection techniques for ERS-1 SAR, *IEEE Trans. Geosci. Remote Sens.* 31:896–906.

Schlesinger, M. E., and Mitchell, J. F. B. (1987), Climate model simulations of the equilibrium climatic response to increased carbon dioxide, *Rev. Geophys.* 25:760–798.

Slaughter, C. W., and Viereck, L. A. (1986), Climatic charac-

teristics of the taiga in interior Alaska, in *Ecological Series Vol. 57, Forest Ecosystems in the Alaskan Taiga* (K. Van Cleve, Ed.), Springer-Verlag, New York, pp. 2–21.

Sturm, M., and Johnson, J. B. (1992), Thermal conductivity measurements of depth hoar, *J. Geophys. Res.* 97(B2):2129–2139.

Trabant, D. C., and Benson, C. S. (1972), Field experiments on the development of depth hoar, in *Studies of Mineralogy and Precambrian Geology* (B. R. Doe, and D. K. Smith, Eds.), Geol. Soc. Am. Mem. 135, pp. 309–322.

Ulaby, F. T., and El-Rayes, M. A. (1987), Microwave dielectric spectrum of vegetation, Part II: Dual-dispersion model, *IEEE Trans. Geosci. Remote Sens.* 25:550–557.

Ulaby, F. T., Moore, R. K., and Fung, A. K. (1986), *Microwave Remote Sensing: Active and Passive. Volume III: From Theory to Applications*, Artech House, Dedham, MA.

Ulaby, F. T., Sarabandi, K., McDonald, K., Whitt, M., and Dobson, D. C. (1990), Michigan microwave canopy scattering model, *Int. J. Remote Sens.* 11:1223–1254.

Van Cleve, K., and Viereck, L. A. (1981), Forest succession in relation to Nutrient cycling in the boreal forest of Alaska, in *Forest Succession: Concepts and Applications* (D. West, et al., Eds.), Advanced Texts in Life Sciences, Springer-Verlag, New York, pp. 185–211.

Viereck, L. A., Dyrness, C. T., Van Cleve, K., and Foote, M. J. (1983), Vegetation, soils, and forest productivity in selected forest types in interior Alaska, *Can. J. For. Res.* 13:703–720.

Way, J. B., Paris, J., Kasischke, E., et al. (1990), The effect of changing environmental conditions on microwave signatures of forest ecosystems: preliminary results of the March 1988 Alaskan aircraft SAR experiment, *Int. J. Remote Sens.* 11:1119–1144.

Wegmüller, U. (1990), The effect of freezing and thawing on the microwave signatures of bare soil, *Remote Sens. Environ.* 33:123–135.